Synthesis and UV absorption properties of 5-sulfosalicylate-intercalated Zn–Al layered double hydroxides

Linyan Zhang, Yanjun Lin, Zhenjun Tuo, David G. Evans, Dianqing Li[*]

State Key Laboratory of Chemical Resource Engineering, Beijing University of Chemical Technology, Beijing 100029, China

Abstract

5-sulfosalicylic acid (SSA) anions have been intercalated into layered double hydroxides (LDHs) by an anion-exchange reaction using ZnAl–NO_3–LDHs as a precursor. The samples were characterized by XRD, FT-IR, TG-DTA/MS and UV–visible spectroscopy. The results show that the NO_3^- anions in the precursor have been completely replaced by SSA anions to give ZnAl–SSA–LDHs having a high degree of crystallinity. Detailed studies reveal the existence of a supramolecular structure in ZnAl–SSA–LDHs involving electrostatic attraction between opposite charges, hydrogen bonding and other weak chemical bonding interactions between host layers and SSA anions. The thermal stability of ZnAl–SSA–LDHs is considerably enhanced compared with that of a mixture of ZnAl–NO_3–LDHs and SSA. After addition of 2.0 wt% ZnAl–SSA–LDHs to polypropylene (PP), the resistance of the polymer to UV degradation is significantly improved.

© 2007 Elsevier Inc. All rights reserved.

Keywords: Layered double hydroxide; 5-sulfosalicylate; Intercalation; Supramolecular structure; UV degradation

1. Introduction

Layered double hydroxides (LDHs) are a well-known type of anionic clay with the general formula $[M_{1-x}^{2+}M_x^{3+}(OH)_2]^{x+}(A_{x/n}^{n-}) \cdot mH_2O$, where M^{2+} and M^{3+} are, respectively, divalent and trivalent metallic cations, x is the molar ratio of $M^{3+}/(M^{2+}+M^{3+})$ and A^{n-} symbolizes various organic or inorganic anions [1,2]. Recently LDHs have attracted increasing attention because of the ready exchangeability of their interlayer anions [3]. By intercalation of appropriate guest anions into the galleries between the host layers, the properties of LDHs can be tailored to give new functional materials which can be used, for example, as catalysts, absorbents, and anionic exchangers [4–7].

5-sulfosalicylic acid (SSA) has the ability to coordinate to Fe^{3+}, Cu^{2+} or other cations giving complexes with different colors, and therefore is often used in the qualitative or quantitative determination of such metallic elements. SSA and its derivatives also show good UV

absorbing capacity; however, their thermal stability is poor which restricts their application in practice. Previous work in our laboratory has shown that the thermal stability of organic anions can be greatly improved by intercalation into LDHs and the layers can be said to act as a "molecular container" for the guest anions [8]. Photo- and thermally stable pigments [9] and UV absorbents [10] have been synthesized in this way.

In this work, we report the synthesis of an organic/inorganic UV absorbing material by intercalation of SSA anions into ZnAl–NO_3–LDHs. A composite film has been prepared by addition of ZnAl–SSA–LDHs powders to polypropylene (PP) resin and the UV resistance capability of this material is also investigated.

2. Experimental section

2.1. Chemicals

NaOH, $Zn(NO_3)_2 \cdot 6H_2O$, $Al(NO_3)_3 \cdot 9H_2O$ and SSA were all of A.R. grade, and were purchased from Beijing Chemical Reagent Company. CO_2-free deionized water

---

*Corresponding author. Fax: +86 10 6442 5385.
  E-mail address: lidq@mail.buct.edu.cn (D. Li).

with conductivity less than $10^{-6}\,S\,cm^{-1}$ was used in synthesis and washing steps. Commercial isotactic PP (1700) was purchased from Yanshan Petrochemical Company (China).

2.2. Preparation of ZnAl–NO₃–LDHs precursor

ZnAl–NO₃–LDHs was prepared using a method involving separate nucleation and aging steps (SNAS) [11]. NaOH (15.36 g, 0.384 mol) was dissolved in CO_2-free deionized water (200 ml) to make an alkali solution. $Zn(NO_3)_2 \cdot 6H_2O$ (47.60 g, 0.160 mol) and $Al(NO_3)_3 \cdot 9H_2O$ (30.01 g, 0.080 mol) were dissolved in CO_2-free deionized water (200 ml) to prepare a mixed salt solution. The two solutions were simultaneously added to a colloid mill reactor with rotor speed of 4000 rpm and the resulting suspensions were subsequently aged at reflux temperature for 6 h under N_2 protection. The precipitate was then filtered and washed until the pH value of the washings was less than 8. The material was stored as a moist filter cake under nitrogen. The solid content of the filter cake was found to be 16.2%.

2.3. Synthesis of ZnAl–SSA–LDHs

ZnAl–SSA–LDHs was prepared by anion-exchange method. SSA (0.672 g, 2.643 mmol) and NaOH (0.211 g, 5.275 mmol) were dissolved in CO_2-free deionized water (150 ml) to make an aqueous solution. An amount of the ZnAl–NO₃–LDHs filter cake (6.973 g, ca. 3.304 mmol of NO_3^-) prepared above was dispersed in CO_2-free deionized water (150 ml) to prepare a suspension which was heated to reflux temperature, after which the solution containing SSA and NaOH was added drop-wise over 2 h with rapid stirring under strict N_2 protection. The pH value after ion-exchange reaction was about 6.5. The resulting slurry was aged at reflux temperature for 6 h. After being washed eight times, the filter cake was dried at $70\,°C$ for 24 h.

2.4. Characterization and analysis

Powder X-ray diffraction patterns of the samples were recorded with a Shimadzu XRD-6000 diffractometer under the following conditions: 40 kV, 30 mA, scan speed of $5\,°\,min^{-1}$, CuKα ($\lambda = 0.15406$ nm) radiation. Fourier transform infrared (FT-IR) spectra were recorded in the range 4000–$400\,cm^{-1}$ on a Bruker Vector 22 Fourier transform spectrometer using the KBr pellet technique (1 mg of sample in 100 mg of KBr). Diffuse reflectance UV–visible spectra were recorded on a Shimadzu UV-2501PC spectrometer equipped with an integrating sphere attachment in the range 200–800 nm using $BaSO_4$ as background. Weight loss and decomposition behavior of the samples were determined using a Perkin Elmer TG-DTA/MS instrument with a heating rate of $10\,°\,min^{-1}$ and flow velocities of N_2 and O_2 being 180 and $50\,ml\,min^{-1}$, respectively. Elemental analysis for metal ions was carried out using a Shimadzu

ICPS-7500 inductively coupled plasma emission spectrometer and the content of carbon and nitrogen was determined using a Carlo Erba 1106 elemental analyzer.

2.5. Preparation of films of ZnAl–SSA–LDHs/PP and pristine PP

ZnAl–SSA–LDHs (2.0 wt%) was thoroughly mixed with PP in an SSR-Z4 double roller mixer for about 15 min at $165\,°C$. The resulting ZnAl–SSA–LDHs/PP composite was molded into flakes of $80 \times 100 \times 1$ mm and films of 0.05 mm thickness were then formed at $160\,°C$ under pressure. The reference films of pristine PP were prepared under the same conditions. Films of a mixture of SSA/PP cannot be prepared because the mixture quickly turns dark when mixed in the double roller mixer at $165\,°C$.

2.6. Photo-stability of ZnAl–SSA–LDHs/PP and pristine PP films

Samples of ZnAl–SSA–LDHs/PP and pristine PP films were photo-aged at $70\,°C$ in a UV photo-aging instrument (ultraviolet high pressure mercury lamp used as UV light source, power of 1000 W and $\lambda_{max} = 365$ nm) with a controllable temperature system. Diffuse reflectance UV–visible spectra were recorded after UV-irradiation for 5 min. The above process was repeated seven times, giving a total of 35 min accumulated exposure for each sample.

3. Results and discussion

3.1. Characterization and analysis of samples

3.1.1. XRD characterization

The XRD pattern of SSA is shown in Fig. 1(a) and that of the ZnAl–NO₃–LDHs precursor, prepared by a method involving SNAS developed in our laboratory, is shown in Fig. 1(b). The three strong diffraction peaks at low angle in the latter pattern are characteristic of a layered structure and correspond to the basal reflection and higher order reflections. The interlayer spacing (d_{003}) is 0.90 nm, which is close to the literature value of 0.88 nm [12]. The strong sharp reflections indicate that the ZnAl–NO₃–LDHs precursor has a well-formed crystalline layered structure. The ZnAl–NO₃–LDHs precursor was reacted with a solution of SSA dissolved in NaOH, with the pH value at the conclusion of the reaction being about 6.5. Under these pH conditions, the SSA is expected to exist as a dianion with the sulfonic acid (strong acid) and carboxylic acid ($pK_a \sim 2.5$) groups being ionized and the hydroxyl group ($pK_a \sim 12$) remaining undissociated. This is confirmed by spectroscopic and analytical data as discussed below. After SSA anions are intercalated into the interlayer galleries of ZnAl–NO₃–LDHs, the diffraction peaks move to lower 2θ angles. This result is expected for LDHs intercalated with large anions. As shown in Fig. 1(c), the new (003), (006) and (009) diffraction peaks at 7.58°, 14.10° and 15.43°,
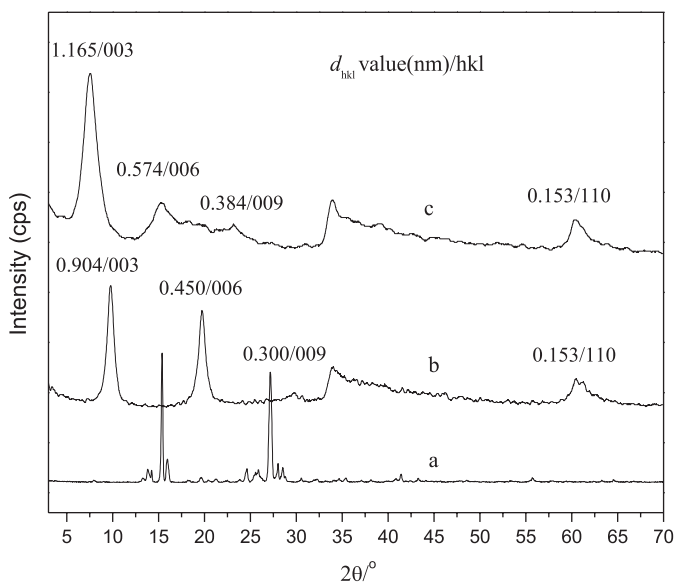
Fig. 1. XRD patterns of SSA (a), ZnAl–NO$_3$–LDHs precursor (b) and ZnAl–SSA–LDHs (c).

Fig. 2. FT-IR spectra of disodium 5-sulfosalicylate (a), ZnAl–NO$_3$–LDHs precursor (b) and ZnAl–SSA–LDHs (c).

Table 1
Indexing of XRD patterns for ZnAl–NO$_3$–LDHs precursor and ZnAl–SSA–LDHs

	ZnAl–NO$_3$–LDHs	ZnAl–SSA–LDHs
d_{003}/nm	0.904	1.165
d_{006}/nm	0.450	0.574
d_{009}/nm	0.300	0.384
d_{110}/nm	0.153	0.153
Lattice parameter a/nm	0.306	0.306
Lattice parameter c/nm	2.712	3.495

corresponding to a basal spacing (d_{003}) of 1.17 nm, indicate that SSA anions have replaced NO$_3^-$ in the interlayer galleries to give ZnAl–SSA–LDHs. Indexation of the XRD patterns for the ZnAl–NO$_3$–LDHs precursor and ZnAl–SSA–LDHs is listed in Table 1.

3.1.2. FT-IR spectroscopy

FT-IR spectra of disodium 5-sulfosalicylate, ZnAl–NO$_3$–LDHs and ZnAl–SSA–LDHs are shown in Fig. 2. The absorption band of disodium 5-sulfosalicylate (Fig. 2a) at 3496 cm^{-1} is assigned to the aromatic C–O–H. Peaks at 1573 and 1376 cm^{-1} are attributed to the ν_{as} and ν_s vibration of –COO$^-$ and the characteristic absorption bands of SO$_3^-$ appear at 1178 and 1040 cm^{-1}. The broad and strong absorption band between 3600 and 3200 cm^{-1} centered at 3454 cm^{-1} in the spectrum of the ZnAl–NO$_3$–LDHs precursor (Fig. 2b) is due to the O–H stretching vibrations of layer hydroxyl groups and inter-layer water molecules [13]. The sharp and narrow absorption band at 1384 cm^{-1} is due to the ν_3 stretching vibration of NO$_3^-$ groups and the band at 427 cm^{-1} is attributed to O–M–O vibrations in the brucite-like layers of LDHs. After the ion-exchange reaction, the ν_{as} and ν_s absorption
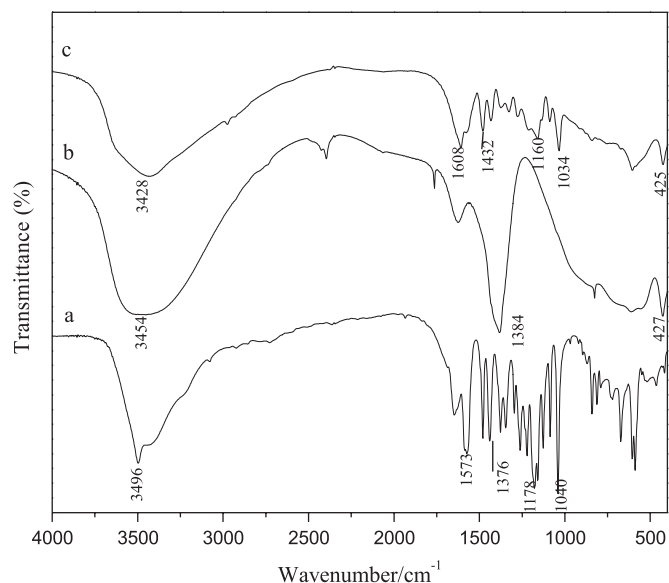
peaks of –COO$^-$ move to 1608 and 1432 cm^{-1}, and the characteristic absorption peaks of SO$_3^-$ move to 1160 and 1034 cm^{-1}. These results indicate that there exist strong electrostatic interactions between the host layers and the guest anions. The absorption band at 1384 cm^{-1} in ZnAl–NO$_3$–LDHs precursor has disappeared, indicating that the interlayer NO$_3^-$ groups have been completely replaced by SSA anions.

3.1.3. TG-DTA/MS analysis

The nature of the interactions between the host layers and guest anions can also be investigated by TG-DTA/MS analysis. Fig. 3a shows the TG-DTA curves of SSA. The endothermic band at 230 °C in the DTA curve corresponds to the loss of crystal water. A small exothermic band at 290 °C can be assigned to the partial decomposition of SSA and the strong exothermic band near 530 °C is attributed to the complete combustion of SSA. These three processes all have their corresponding weight loss stages in the TG curve. As shown in Fig. 3b, the DTA curve of ZnAl–NO$_3$–LDHs precursor has a large endothermic peak near 250 °C with a corresponding weight loss in the TG curve between 100 and 260 °C. This is due to the removal of interlayer water. With increasing temperature, there are two weight loss stages in the range 260–480 and 480–575 °C in the TG curve, which can be attributed to the removal of layer hydroxyl and NO$_3^-$ groups [14]. The DTA curve of ZnAl–SSA–LDHs shown in Fig. 3c has an obvious endothermic band and a strong exothermic band. The endothermic band in the range 70–460 °C centered at 280 °C in the DTA curve is attributed to the removal of the small amount of physically adsorbed water and the interlayer water and the layer hydroxyl groups. The strong exothermic band near 560 °C is assigned to the complete combustion of SSA anions. The corresponding TG curve
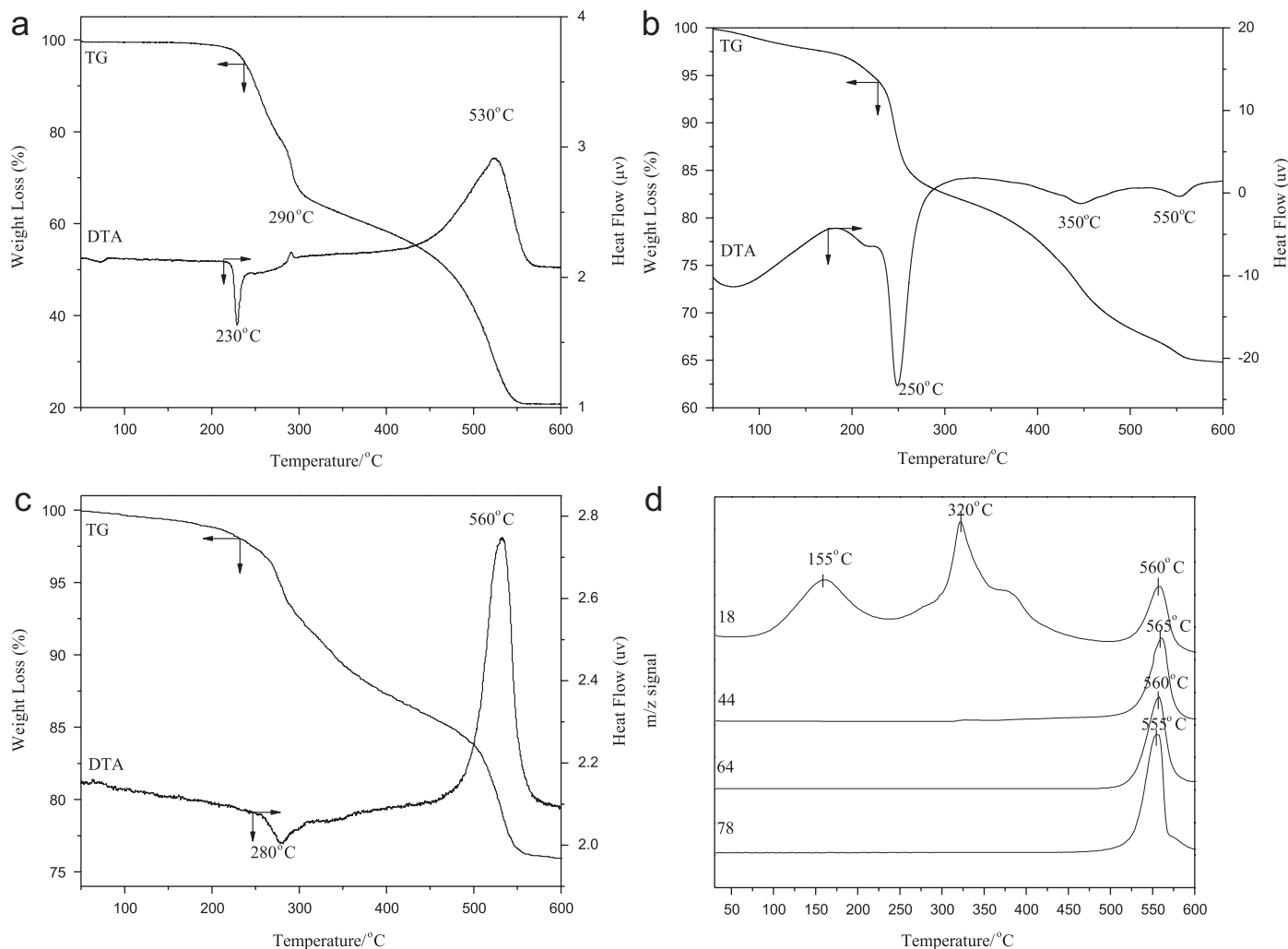
Fig. 3. TG-DTA curves of SSA (a), ZnAl–NO$_3$–LDHs precursor (b) and ZnAl–SSA–LDHs (c) and TG/MS curves of ZnAl–SSA–LDHs (d).

Table 2
Chemical compositions of the ZnAl–NO$_3$–LDHs precursor and ZnAl–SSA–LDHs

Sample	Zn (wt%)	Al (wt%)	N (wt%)	C (wt%)	Zn/Al molar ratio	Formula
ZnAl–NO$_3$–LDHs	32.73	6.93	4.61	—	1.95	Zn$_{0.66}$Al$_{0.34}$(OH)$_2$(NO$_3$)$_{0.34}$·0.49H$_2$O
ZnAl–SSA–LDHs	29.51	6.77	—	10.01	1.80	Zn$_{0.64}$Al$_{0.36}$(OH)$_2$[O–HO(C$_6$H$_3$)COOSO$_3$]$_{0.18}$·0.50H$_2$O

shows two weight loss stages. The mass spectra shown in Fig. 3d allow a detailed analysis of the thermal decomposition behavior of ZnAl–SSA–LDHs. A small amount of physically adsorbed water and interlayer water is released from 70 to 230 °C. The removal of layer hydroxyl groups occurs between 230 and 460 °C. The decomposition and combustion of SSA anions take place in the temperature range 450–600 °C, releasing H$_2$O, CO$_2$, SO$_2$ and benzene. It can be concluded from the TG-DTA/MS analysis that the thermal stability of SSA has been enhanced to some extent after intercalation into ZnAl–NO$_3$–LDHs.

The TG-DTA/MS analysis results are therefore consistent with the FT-IR data and suggest that ZnAl–SSA–LDHs is characterized by an array of supramolecular interactions between host layers and guest anions and that

the material does not behave as a simple mixture of SSA and ZnAl–NO$_3$–LDHs. These interactions between host layers and guest anions involve electrostatic attraction between opposite charges, hydrogen bonding and van der Waals forces.

3.1.4. Elemental analysis

The results of elemental analysis and the calculated structural formulae of the ZnAl–NO$_3$–LDHs precursor and ZnAl–SSA–LDHs are listed in Table 2. The quantities of water were estimated from the TG data. The results confirm that the nitrate anions in the precursor have been completely replaced by SSA anions. The molar ratio of elements in the layers shows little change indicating that

there is no destruction of the layers during the intercalation process.

3.2. Photochemical properties of samples

3.2.1. UV–visible absorbance curves of samples

UV–visible absorbance curves of SSA, ZnAl–NO$_3$–LDHs and ZnAl–SSA–LDHs are shown in Fig. 4. The curve for ZnAl–NO$_3$–LDHs (Fig. 4b) shows strong UV absorption at 220 and 300 nm, which is attributed to the presence of nitrate anions in the interlayer galleries [15]. These two absorption peaks disappear after SSA is intercalated into ZnAl–NO$_3$–LDHs precursor while the absorption in the ultraviolet area becomes more intense than in SSA itself (Fig. 4a). The UV absorbance between 250 and 350 nm exceeds 80% and is nearly 90% at 335 nm, showing that the material has excellent potential as a practical UV absorbing agent. From Fig. 4 it can be seen that ZnAl–SSA–LDHs has an additional absorption between 400 and 500 nm, whereas the SSA and ZnAl–NO$_3$–LDHs precursors are transparent in this region. This can be ascribed to supramolecular guest–guest or guest–host interactions and supports the suggestion (see Section 3.1.3) that the material does not behave as a simple mixture of SSA and ZnAl–NO$_3$–LDHs.

3.2.2. Photo-stability of film samples

The photo-oxidative degradation mechanism of PP has been studied by IR spectroscopy [16,17]. The decomposition product shows two characteristic absorption peaks associated with carbonyl and hydroxyl groups at 1716 and 3411 cm^{-1}, respectively. On exposure to UV light, the absorption intensities at 1716 and 3411 cm^{-1} (relative to that of the peak at 841 cm^{-1} due to the C–H out-of-plane deformation as an internal standard) show a gradual increase. In order to study the effect of ZnAl–SSA–LDHs on the degradation of PP, 2.0 wt% of the material was
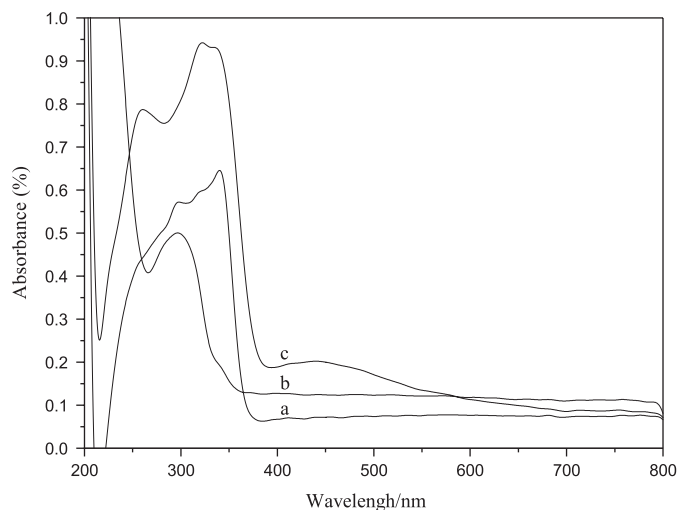
thoroughly mixed with PP resin and pressed into films having 0.05 mm thickness. FT-IR spectra of the ZnAl–SSA–LDHs/PP film and pristine PP film were recorded every five minutes after UV irradiation. The total irradiation time was 35 min. The FT-IR results are shown in Fig. 5. The intensities of the carbonyl absorption peak at 1716 cm^{-1} and the hydroxyl absorption peak at 3411 cm^{-1} in the spectra of ZnAl–SSA–LDHs/PP increase more slowly with time than is the case for pristine PP with the same exposure time to UV irradiation. This can be seen more clearly in Fig. 6, where the intensity ratios $I_{(carbonyl)}/I_{(C–H)}$ and $I_{(hydroxyl)}/I_{(C–H)}$ for ZnAl–SSA–LDHs/PP are plotted against aging time. These results indicate that the

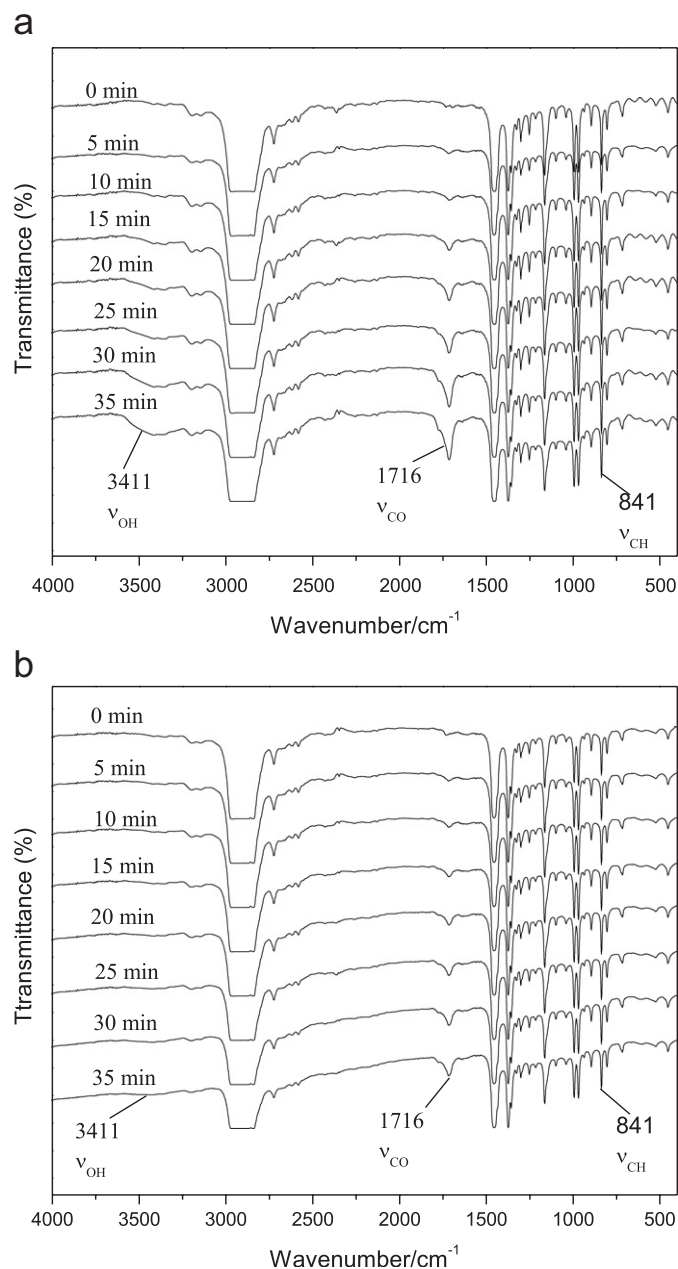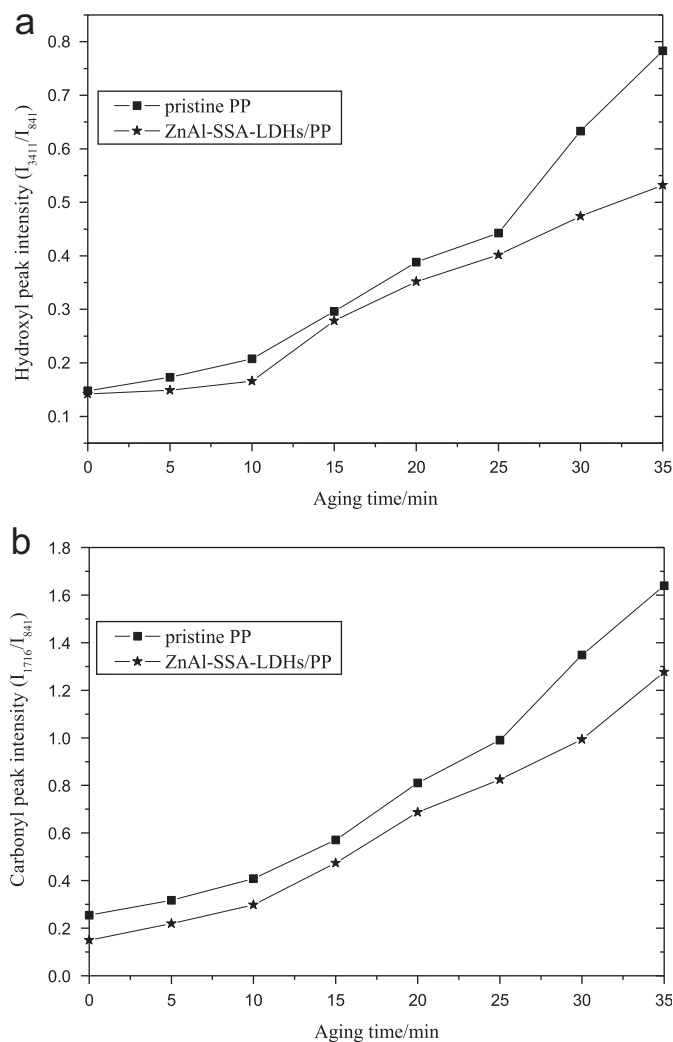Fig. 5. FT-IR spectra of pristine PP (a) and ZnAl–SSA–LDHs/PP (b) films after different UV exposure times.

Fig. 4. UV–visible absorbance spectra of SSA (a), ZnAl–NO$_3$–LDHs precursor (b) and ZnAl–SSA–LDHs (c).

Fig. 6. Intensity ratios I (hydroxyl)/I (C–H) (a) and I (carbonyl)/I (C–H) (b) of pristine PP and ZnAl–SSA–LDHs/PP films after different UV exposure times.

UV resistance capacity of PP has been improved by the addition of ZnAl–SSA–LDHs, and therefore the aging of PP is markedly inhibited.

4. Conclusions

5-sulfosalicylic acid (SSA) anions have been successfully intercalated into the interlayer galleries of LDHs by an anion-exchange reaction using ZnAl–NO₃–LDHs as precursor. XRD results show that the basal spacing increases from 0.90 nm in the precursor to 1.17 nm for ZnAl–SSA–LDHs.

FT-IR, TG-DTA/MS and UV–visible spectroscopy results indicate that there exists a complex system of supramolecular interactions between the host layers and the guests in ZnAl–SSA–LDHs, which enhance the thermal stability of ZnAl–SSA–LDHs relative to that of the LDH precursor and SSA itself. The temperature of interlayer water removal for ZnAl–SSA–LDHs and the decomposition temperature of interlayer SSA anions are both increased by about 30 °C relative to the corresponding values for the LDH precursor and SSA, respectively.

UV–visible spectroscopy also shows that the UV absorption of ZnAl–SSA–LDHs is higher than both the ZnAl–NO₃–LDHs precursor and SSA. The absorbance between 250 and 350 nm exceeds 80% while the value at 335 nm reaches nearly 90%. After addition of 2.0 wt% ZnAl–SSA–LDHs, the UV resistance capability of PP is significantly enhanced as measured by FT-IR spectroscopy using an internal standard method.

References

[1] F. Cavani, F. Trifiro, A. Vaccari, Catal. Today. 11 (1991) 173.
[2] D.G. Evans, R.C.T. Slade, Struct. Bond. 119 (2006) 1.
[3] J. He, M. Wei, B. Li, Y. Kang, D.G. Evans, X. Duan, Struct. Bond. 119 (2006) 89.
[4] H. Tagaya, A. Ogata, T. Kuwahara, S. Ogata, M. Karasu, J. Kadokawa, Micropor. Mater. 7 (1996) 151.
[5] L. Ven der Ven, M.L.M. Van Gernert, L.F. Batenburg, J.J. Keern, L.H. Gielgens, T.P.M. Koster, Appl.Clay Sci. 17 (2000) 25.
[6] F. Li, X. Duan, Struct. Bond. 119 (2006) 193.
[7] D.G. Evans, X. Duan, Chem. Commun. 6 (2006) 485.
[8] Q. Yuan, M. Wei, D.G. Evans, Z. Wang, X. Duan, J. Mater. Chem. 15 (2005) 1197.
[9] S. Guo, D. Li, W. Zhang, M. Pu, D.G. Evans, X. Duan, J. Solid State Chem. 177 (2004) 4597.
[10] S. Miyata, M. Kuroda, US Patent, 1981, US4299759.
[11] Y. Feng, D. Li, C. Li, Z. Wang, D.G. Evans, X. Duan, Clays Clay Miner. 51 (2003) 566.
[12] Q. He, S. Yin, T. Sato, Chem. Solids 65 (2004) 395.
[13] J. Wang, M. Wei, G. Rao, D.G. Evans, X. Duan, J. Solid State Chem. 177 (2004) 366.
[14] D. Li, Z. Tuo, D.G. Evans, X. Duan, J. Solid State Chem. 179 (2006) 3114.
[15] J. Mack, J.R. Boltom, J. Photochem. Photobiol. A: Chem. 128 (1999) 1.
[16] D. Ramkumar, M. Bhattacharya, U. Vaidya, Eur. Polym. J. 33 (1997) 729.
[17] P. He, Y. Xiao, P. Zhang, C. Xing, N. Zhu, X. Zhu, D. Yan, Polym. Degrad. Stab. 88 (2005) 473.